Submitted to the Journal of Electroanalytical Chemistry, November 6, 2002

Surface Segregation Effects in Electrocatalysis: Kinetics of Oxygen Reduction Reaction on Polycrystalline Pt_3Ni Alloy Surfaces**

V. Stamenković*, T.J. Schmidt[1)], P.N. Ross and N.M. Marković

Materials Sciences Division, Lawrence Berkeley National Laboratory

University of California at Berkeley, CA 94720, USA

Abstract

Effects of surface segregation on the oxygen reduction reaction (ORR) have been studied on a polycrystalline Pt_3Ni alloy in acid electrolyte using ultra high vacuum (UHV) surface sensitive probes and the rotating ring disk electrode (RRDE) method. Preparation, modification and characterization of alloy surfaces were done in ultra high vacuum (UHV). Depending on the preparation method, two different surface compositions of the Pt_3Ni alloy are produced: a sputtered surface with 75 % Pt and an annealed surface (950 K) with 100 % Pt. The latter surface is designated as the "Pt-skin" structure, and is a consequence of surface segregation, *i.e.,* replacement of Ni with Pt atoms in the first few atomic layers. Definitive surface compositions were established by low energy ion scattering spectroscopy (LEISS). The cyclic voltammetry of the "Pt-skin" surface as well as the pseudcapacitance in the hydrogen adsorption/desorption potential region is similar to a polycrystalline Pt electrode. Activities of ORR on Pt_3Ni alloy surfaces were compared to polycrystalline Pt in 0.1M $HClO_4$ electrolyte for the observed temperature range of $293 < T < 333$ K. The order of activities at 333 K was: "Pt-skin" > Pt_3Ni (75% Pt) > Pt with the maximum catalytic enhancement obtained for the "Pt-skin" being 4 times

that for pure Pt. Catalytic improvement of the ORR on Pt_3Ni and "Pt-skin" surfaces was assigned to the inhibition of Pt-OH_{ad} formation (*on* Pt sites) versus polycrystalline Pt. Production of H_2O_2 on both surfaces were similar compared to the pure Pt. Kinetic analyses of RRDE data confirmed that kinetic parameters for the ORR on the Pt_3Ni and "Pt-skin" surfaces are the same as on pure Pt: reaction order, m=1, two identical Tafel slopes, activation energy, ≈ 21-25 kJ/mol. Therefore the reaction mechanism on both Pt_3Ni and "Pt-skin" surfaces is the *same* as one proposed for pure Pt *i.e.* $4e^-$ reduction pathway.

Keywords: surface segregation, electrocatalysis, alloys, platinum nickel, oxygen reduction reaction, surface composition

**Dedicated to Michael J.Weaver's contribution to electrochemistry

*corresponding author: vrstamenkovic@lbl.gov

[1)] present address: Celanese Ventures GmbH, D-65926 Frankfurt, Germany

1. Introduction

Surface segregation on alloys has been intensively studied in the past few decades. According to the recent research, surface segregation, *i.e.* the enrichment of one element at the surface relative to the bulk, is a general phenomenon observed from the experimental studies of various bimetal alloys [1]. This topic has drawn much scientific attention mainly because of direct influence to technology-related physical and chemical properties of surfaces such as electronic, magnetic, corrosive resistance as well as catalytic properties, etc. However, aside from a very few reports [2-5], surface segregation has been an entirely neglected phenomenon in a large number of studies on alloys and other bimetallic surfaces in an electrochemical environment.

The details of segregation are still not completely understood and they are also subject of many theoretical considerations [6], especially in the case of segregation on nanoparticles which may differ from that of their bulk analog [7;8]. This is to be expected since the nanoclusters represent a finite quantity of material, so there is no infinite source/sink of constitute atoms and hence material balance constraints become important. All of these complexities and uncertainties on high surface area bimetallic catalysts reinforces the need for using well-characterized materials to identify the fundamental mechanisms at work in the electrocatalysis of the fuel cell reactions. Recently, in our laboratory we reported [9] a detailed comparison of the kinetics of the ORR on bulk alloys of Pt_3Co and on the so-called "Pt_skin" structure that was produced by an exchange of Pt and Co in the first few layers. The LEISS studies revealed that for a polycrystalline Pt_3Co alloy the outermost layer of the clean annealed surface is pure Pt, with Pt depletion in the second layer. It was found that the ORR is uniquely active on the latter surface, the rate of reaction being 4 times that for pure Pt.

In this article we report a related detailed investigation of ORR catalytic activity on Pt_3Ni surfaces, focusing on the properties of the "Pt-skin" in oxygen electrochemistry. All surfaces were

UHV prepared (annealing and sputtering cycles) and characterized (AES and LEISS). Emphasis is placed on a description of alloy surface preparation and characterization procedure as well as on kinetic studies of the ORR. It will be demonstrated that the ability to make a controlled and well characterized arrangement of the two elements in the electrode surface region is essential to the kinetic activities.

2. Experimental

2.1. Surface preparation and characterization

The polycrystalline bulk Pt_3Ni alloy electrode used in this studies was prepared by conventional metallurgy. Bulk composition ($x_{Ni,b}$) was assessed via x-ray fluorescence spectroscopy ($x_{Ni,b} \approx 0.75$); x-ray diffraction showed all specimens to be single-phase *fcc* solid solutions of Pt and Ni having the expected lattice constant for 75 % Pt [10]. Cleaning, modification and surface characterization procedure were performed in UHV system, under base pressure in the $1 \cdot 10^{-10}$ Torr range, which is equipped with an angular-resolving double pass cylindrical mirror analyzer PHI-DPCMA Φ15-255GAR with an electron source at its center. UHV cleaning procedure were done by repeating of sputtering-annealing cycles with Ar^+ and oxygen until Auger electron spectroscopy (AES) indicated that perfectly clean (carbon and oxygen free) surface was produced. AES spectra were recorded in derivative mode using the 3 keV electron beam energy, 3 eV_{p-p} modulation and –5 μA beam current in the range from 140 to 900 eV.

In order to produce a different surface composition, clean samples were either annealed at 950 K or mildly sputtered with 0.5 keV beam of Ar^+ ions. The surface composition of alloy samples were determined by low energy ion scattering spectroscopy (LEISS). A compilation of surfaces analyzed by LEISS has been made by Watson [11]. LEISS spectra were taken with Ne^+

beam energy of 1 keV with sample currents from 5 to 30 nA at residual Ne pressure of $2.5 \cdot 10^{-8}$ Torr. Scattering angle was 127°, and the incidence angle was 45°. A Φ04-303A differentially pumped ion gun was used to raster the Ne^+ ion beam over approximately 3 mm×3 mm surface area. Time of recording was 60 s/spectrum. The clean Pt reference sample was prepared in the same manner. i.e. conventional metallurgy and pre-treated in UHV in exact the same way, mild sputter cleaning and/or annealing.

2.2 Electrochemical measurements

The UHV prepared and characterized alloy surfaces were withdrawn form the UHV introductory port (back-field with argon) into air and covered immediately with a drop of triply pyro-distilled water, for details see [12]. The electrodes were then mounted in a rotating ring disk electrode setup and finally immersed into the electrolyte under potential control at ~0.05V vs RHE in 0.1M $HClO_4$ (Baker, Ultrex). Electrolytes were prepared with triple pyro-distilled water and thermostated at 293, 303, 313 and 333°K, by a circulating constant temperature bath connected to the water jacket of a standard three compartment electrochemical cell. The reference electrode was a saturated calomel electrode (SCE) separated by a bridge from the reference compartment. All potentials in this paper are, however, referenced to the reversible hydrogen electrode potential (RHE) at the same temperature (calibrated from hydrogen oxidation reaction [13]) in the same electrolyte; argon, oxygen and hydrogen were bubbled through a glass frit (Air Products, 5N8 purity). During measuring the polarization curves for the ORR on the disk electrode the ring electrode was potentiostated at 1.15 V, a potential where peroxide oxidation reaction is under pure diffusion control; the collection efficiency *N* for the ring-disk assembly is *ca*. 0.2. The geometrical surface area of the disk electrode was 0.283 cm^2, and all voltammograms were recorded with a sweep rate of 50 mV/s.

3. Results and Discussion

3.1 Surface Composition

A number of studies have focused on single-crystal Pt based alloys, predominantly on Pt-TM surfaces (TM refer to transition metals) . At the present time the quantitative low energy electron diffraction (LEED) intensity results obtained by the Grenoble group [14] appears to be the most notable source of information on the Pt-TM (TM=Ni, Co, Fe) surfaces with layer by layer resolution. As revealed from these LEED studies, $Pt_{78}Ni_{22}$(111) [15], $Pt_{80}Co_{20}$(001) [16], $Pt_{80}Co_{20}$(111) [17], $Pt_{80}Fe_{20}$(111) [18] and Pt_xRh_{1-x}(hkl) [19;20] alloys all exhibit compositional oscillations of alloying components in the first three atomic layers. For most (111) and (100) crystals, the outermost layer of the clean, annealed surfaces are *pure* Pt, which we shall call hereafter the "skin" structure, with Pt depletion in the second layer. It has been found that at least some catalytic properties of the "Pt-skin" structures in UHV are different from the pure Pt surface [16;21]. This was attributed to the electronic effect of intermetallic bonding of the alloying component-rich second layer with the top-most Pt atoms.

In our experiments corresponding AES spectra of Pt_3Ni polycrystalline surfaces, obtained after either mild sputtering or annealing of specimens, are shown in Figure 1 a). The AES confirmed that after sputtering or annealing cycles both alloy surfaces were clean, showing characteristic Pt (158, 168, 189, 199, 237, 251, 390 eV) and Ni (716, 783, 848 eV) peaks, respectively. By comparison of both AES spectra, no shift of any peak was observed but significant change of the peak intensities has been found for the both elements. Annealed surface showed decrease of all three Ni peak intensities and increase of Pt peaks. That was first indication that the surface segregation of Pt occurs on the polycrystalline Pt_3Ni alloy. Quantitative surface analysis of the Pt_3Ni alloy with AES is quite complicated, requiring modeling of emission from several subsurface layers with dynamical scattering of the outgoing Auger electron. Because the

contribution of Auger emission from the several atomic layers in the Pt_3Ni alloy causes the Pt/Ni AES ratio to be much different than the ratio would be with emission only from the first layer, AES has only been used to verify the cleanliness of alloy surfaces. In contrast, the most accurate surface composition of outermost atomic layers of the Pt_3Ni alloy were obtained by optimizing LEISS, which is a more surface specific technique and more useful for segregation studies. The LEISS results are shown in Figure 1b), where the positions of the scattering peaks of the Pt and Ni are calculated from the classical equation for elastic collisions [22]. The data, obtained by 1 keV Ne^+ beam, showed that the outermost atomic layer after annealing at 950 K contains only Pt atoms, confirming that the "Pt-skin" structure can also be created on Pt_3Ni alloy.

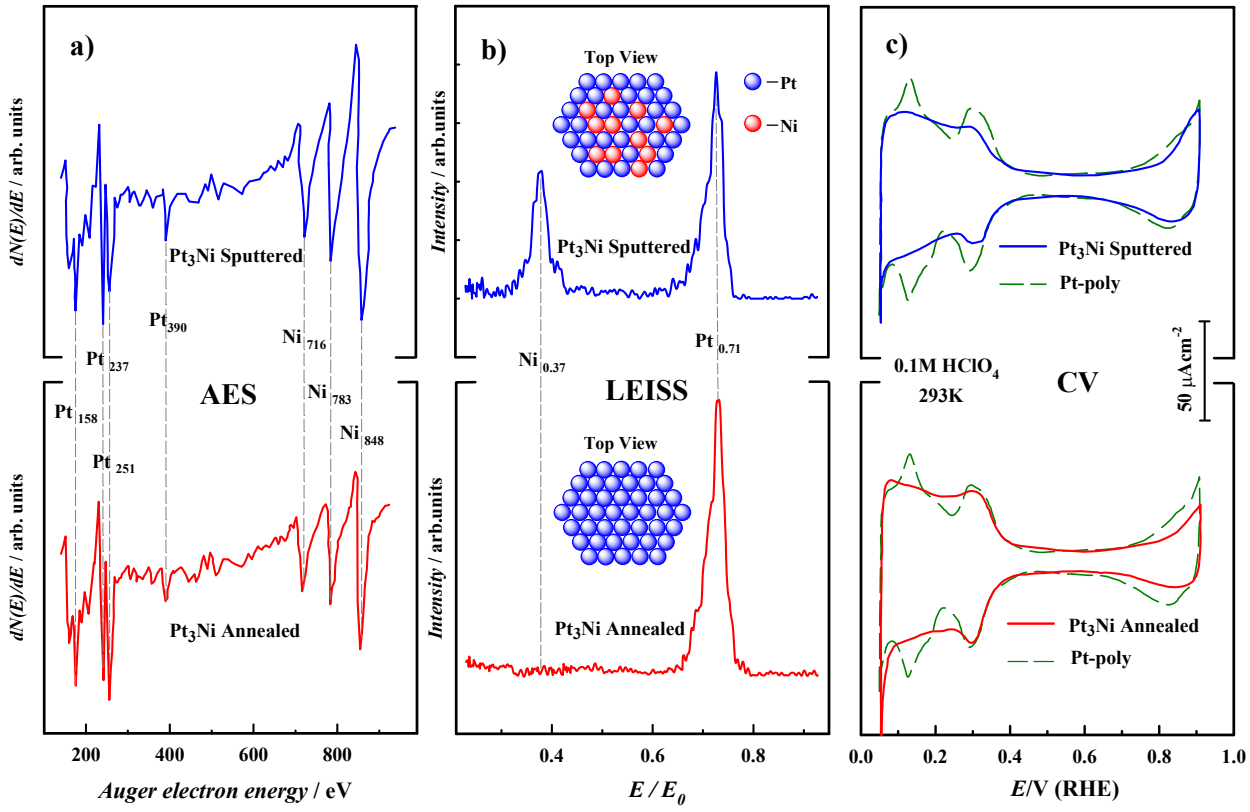

Figure 1. **a)** Auger electron spectroscopy of annealed and mildly sputtered Pt_3Ni. **b)** Low energy ion scattering spectra of the same two surfaces. Also shown is schematic picture of the "Pt-skin" electrode and the sputtered Pt_3Ni electrode. **c)** Cyclic voltammetry (sweep rate 50mV/s) of Pt: and Pt_3Ni surface at 293 K (upper curves), and "Pt-skin" surface (lower curves) in 0.1 M $HClO_4$.

The LEISS spectra taken after mild sputtering revealed that also Ni atoms are present in the outermost layer of the clean sputtered surface. Using the elemental sensitivity factors of polycrystalline materials [23], surface composition is estimated to 75% of Pt and 25% of Ni, equal to the bulk concentration of the Pt_3Ni alloy. Both annealed and sputtered specimens were transferred into the electrochemical cell for electrochemical characterization.

3.2 Cyclic Voltammetry

Cyclic voltammograms of sputtered Pt_3Ni, "Pt-skin" and polycrystalline Pt electrodes recorded in argon purged 0.1 M $HClO_4$ at 293K are shown in Figure 1c). Two general features emerge from cyclic voltammetry:

(i) in the hydrogen adsorption potential region ($0 < E < 0.4$ V), the underpotential deposition of hydrogen (H_{upd}) is accompanied by rather weak desorption/adsorption of anions of the supporting electrolyte, which on Pt produces two pronounced peaks located at 0.15 and 0.3 V. Notice that neither Pt_3Ni nor "Pt-skin" electrodes exhibit the sharp peak at ca. 0.15 V, suggesting that the adsorption of anions on these two bimetallic surfaces is different than on pure Pt. In addition, the total charge under the H_{upd} region is significantly different on Pt_3Ni versus Pt, e.g. 165 $\mu C/cm^2$ on the sputtered surface versus 208 $\mu C/cm^2$ on polycrystalline Pt electrode. Thus, the charge for the H_{upd} adsorption on the former surface is reduced by ca. 25% from the charge required to form a monolayer of H_{upd}, or simply by the amount of Ni atoms present in the surface (from LEISS data ca.25at%). This is confirmation for our previous suggestion that H_{upd} is not adsorbed on Ni atoms. In contrast to Pt_3Ni, however, the total charge which corresponds to the adsorption of H_{upd} on the "Pt-skin" electrode (ca. 205 $\mu C/cm^2$) and Pt is almost identical, suggesting that indeed the surface of the annealed electrode exclusively contains the layer ("skin") of Pt surface atoms.

ii) the oxide formation ($E >$ ca.0.7 V) is strongly affected by the nature of surface atoms. As shown in Figure 1 c), the onset of oxide formation shifts towards more positive potentials on Pt_3Ni

surface, suggesting that alloying with Ni effects a fundamental change in the way Pt atoms interact with H_2O and anions of supporting electrolyte. For the annealed surface, that shift is even more pronounced, which in turn produced a significantly lower oxide coverage at he same potential, *e.g.*, 0.9 V. In the subsequent section, we will show that this is the key to understanding high catalytic activity of the Pt_3Ni and Pt-skin electrodes.

Cyclic voltammetry of all electrodes recorded above room temperature (not shown) were very similar to those observed at 293 K, providing a good accordance with the previous observation that temperature, in the given range of 293-333 K, has rather small effect on the voltammetric features of polycrystalline Pt and Pt single crystals in either acid [13;24] or alkaline [25] solutions. All voltammetric features shown in Figure 1 c) were reproduced in the consecutive scans and the voltammetry remained stable at all temperatures ($293 < T < 333$ K), confirming that during the experiment (including the measurements of ORR kinetics) there was no corrosion/dissolution of alloying component - Ni.

3.3 Oxygen Reduction Kinetics

A characteristic set of polarization curves for the ORR on the annealed Pt_3Ni alloy in 0.1 M $HClO_4$ at 298 K along with the kinetic analyses, presented in the form of the Tafel plot (insert b) of mass-transport corrected currents (see Eq. 2) and the Levich-Koutecky plots (insert c), are shown in Figure 2. Well defined diffusion limiting currents (j_d) for the ORR (0.2 to 0.7 V) are followed by a region under mixed kinetic-diffusion control, between $0.8 < E < 1.0$ V. Figure 2 provides that in both potential regions the ring currents (I_r) are a rather small fraction of j_d, revealing that the ORR proceeds almost entirely through a $4e^-$ reduction pathway. Increase of peroxide oxidation currents is merged with the adsorption of hydrogen ($E < 0.2$ V), approaching the maximum of ca. 20% at 0.075V. Quantitative presentation of the peroxide production (current efficiency) was calculated from Eq. 1 [26]:

$$x_{H_2O_2} = \frac{2\,I_r/N}{j_d + I_r/N} \qquad (1)$$

where N is the collection efficiency of the ring-disk electrode. In agreement with cyclic voltammetry measurements, in consecutive potential cycles both j_d and I_r remain the same, confirming that all surface compositions of Pt_3Ni alloy were stable during the ORR characterization.

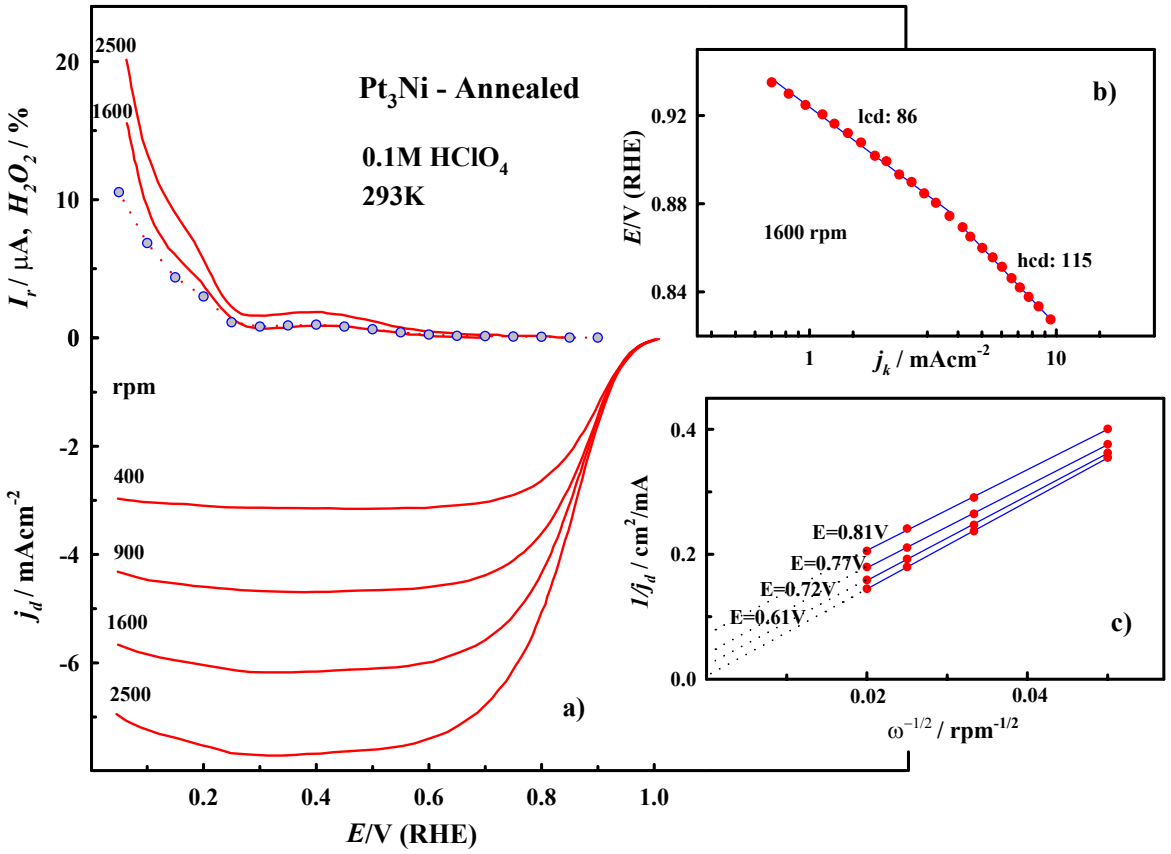

Figure 2. a) Disk (j_d) and ring (I_r) currents (anodic sweep direction) during the ORR on sputtered Pt_3Ni in 0.1 M $HClO_4$ at a sweep rate of 50 mV/s; Ring potential, E=1.15 V; Collection efficiency: N=0.2. **b)** Tafel plot at 1600 rpm. **c)** Levich plot at various electrode potentials.

Tafel plot obtained from the potentiodynamic measurements illustrated in Fig 2 a) is given in Figure 2 b). The polarization curve was fitted with two tangents through the points of whatappear to be a continuous curve. This corresponds to two Tafel slopes; ca. 85 mV/dec for

E > 87 V and ca. 115 mV/dec for E < 0.87 V. As will be discussed latter the change of the Tafel slope appears to be related to the change in the nature of adsorbed oxygen-containing species with potential, a transition that strongly affects the ORR [27-32].

Figure 2 c) shows the so called Levich-Koutecky plot, Eq.2:

$$\frac{1}{j} = \left(\frac{1}{j_k} + \frac{1}{j_d}\right) = f\left(\omega^{-1/2}\right)_E \qquad (2)$$

where for various potentials yields (E) and applied rotational rates (ω), each straight line intercept corresponding to the kinetic current, j_k. Intercept gives the order of absolute kinetic activity of the Pt_3Ni surface for the ORR. In addition, the slope of the straight lines, the so-called "B-factor", allows to estimate the number of electrons involved in the ORR. The experimental value of ca. $4.28 \cdot 10^{-2}$ mA $rpm^{0.5}$ obtained from Figure 2 c) is in a good agreement with the theoretical value of $4.27 \cdot 10^{-2}$ mA $rpm^{0.5}$, calculated for the four electron process from the Levich equation [33], using a literature data for oxygen solubility [34;35], c_0 (c_0=$1.26 \cdot 10^{-3}$ $molL^{-1}$), oxygen diffusivity [36], D (D=$1.93 \cdot 10^{-5}$ cm^2s^{-1}), and kinematic viscosity of the electrolyte [34], ν (ν=$1.009 \cdot 10^{-2}$ cm^2s^{-1}). The linearity of the plots in Figure 2 c) implies a first-order dependence of O_2 kinetics on the annealed surface of Pt_3Ni alloy (100% Pt in the surface). The reaction order (m) was checked further from $log\, j$ vs. $log[(j\text{-}j/j_d)]$ functionality (not shown) using data from Figure 2 c), for details see ref. [37]. The value of m=1.09 was obtained, confirming first order dependence of the kinetics of ORR on the annealed Pt_3Ni surface. Important kinetic parameters for the ORR on Pt-poly, sputtered Pt_3Ni, and the "Pt-skin" surfaces at two temperatures, obtained by using the same methodology as described above, are listed in Table 1. For completeness, the kinetic parameters for the ORR on Pt_3Co surfaces [9] are also included in Table 1.

Potentiodynamic polarization curves for the ORR in 0.1 M $HClO_4$ on Pt and Pt_3Ni surfaces obtained at 293 and 333 K from measurements on all surfaces at 1600 rpm, are shown in Figure 3.

Corresponding curves for the pure Pt in both electrolytes are given as a reference marked with doted lines.

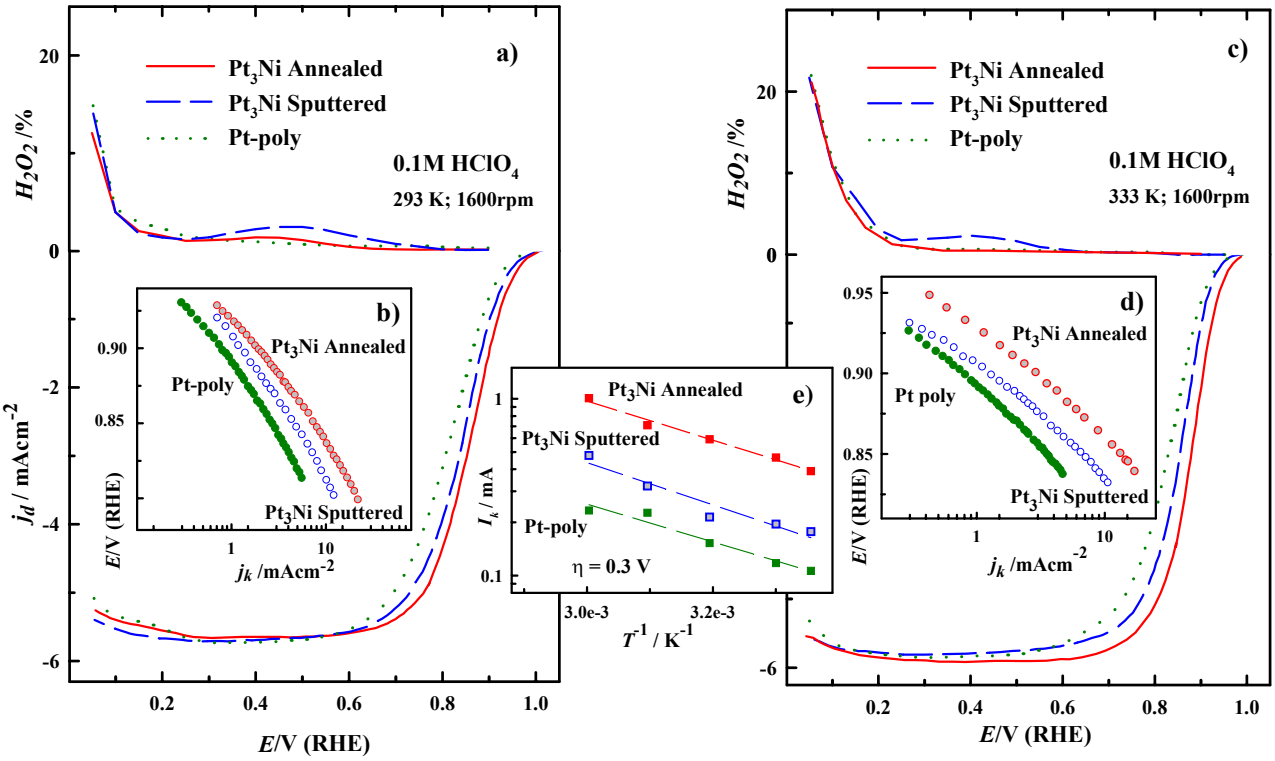

Figure 3. **a)** Disk (j_d) and ring (I_r) currents (anodic sweep direction) during the ORR on Pt, Pt_3Ni and "Pt-skin" surfaces in 0.1 M $HClO_4$ at 293 K. **Insert b:** Tafel plots for all three surfaces at 293 K. **c)** Disk (j_d) and ring (I_r) currents (anodic sweep direction) during the ORR on Pt, Pt_3Ni and "Pt-skin" in 0.1 M $HClO_4$ at 333 K. **Insert d:** Tafel plots for all three surfaces at 333 K. Sweep rate: 50 mV/s; Ring potential, E=1.15 V; Collection efficiency: N=0.2. **Insert e:** Arrhenious plots at overpotential of η=0.3 V for the ORR on Pt, Pt_3Ni and "Pt-skin" surfaces.

In the potential region of $0.05 < E < 1$ V similarly small amounts of H_2O_2 are detected on the ring electrode on all three surfaces at 293 K, implying that, even though Pt_3Ni electrodes are more active than Pt, the reaction pathway of the ORR on Pt alloys may be the same as for a pure Pt electrode. At higher temperatures (Figures 3 c) the polarization curves are qualitatively similar to the curves recorded at room temperature, having the same order of activity as at 293 K. Some negligible increase of peroxide production is observed in diffusion limiting currents region, but in mixed region as well as in H_{upd} region H_2O_2 currents were essentially the same as for the Pt-poly surface.

Close inspection of Figure 3 unambiguously shows that the "Pt-skin" electrode (annealed surface) is the most active surface for the ORR, which is in excellent agreement with previously published data for the "Pt-skin" created on the Pt_3Co alloy surface [9]. That is additional proof that uniform monoatomic layer of Pt surface atoms, which is formed over the Pt depleted and Ni (or Co) enriched second layer, has improved catalytic properties. These results also confirm that the kinetics of the ORR are dependent not only on the nature of alloying component ($Pt < Pt_3Ni < Pt_3Co$) but also on the exact arrangement of the alloying element in the surface region ($Pt_{bulk} < Pt_3Ni < Pt_3Co <$ "Pt-skin" on Pt_3Ni or Pt_3Co) making the surface segregation phenomena a very important factor in supported catalyst synthesis.

The effect of temperature on the ORR rate is shown in Figure 3. The enhancement in the ORR rate at 333 K is rather small (less than factor of 2), reflecting that the temperature dependence of the chemical rate constant is not significant, *i.e.*, the chemical constant is approximately proportional to the $exp(-\Delta H^{\neq}/kT)$ term, where $\Delta H^{\neq}$ is the apparent enthalpy of activation (termed as the activation energy), k is the Boltzman constant and R is the universal gas constant. The activation energies are evaluated for the fixed overpotential at η=0.3 V using the Arrhenius equation:

$$\left.\frac{\partial\left(\log j_k\right)}{\partial\left(1/T\right)}\right|_{\eta} = \frac{\Delta H^{\neq}}{2.3 \cdot R} \qquad (3)$$

Insert e) in Figure 3 shows the Arrhenius plots of three different surfaces. The activation energies determined from the least square regressions were essentially identical on polycrystalline Pt, Pt_3Ni and the "Pt-skin" covering the range between 20-23 kJ/mol, see Table 1. These values are in close agreement with values reported for single crystal platinum electrodes [38], polycrystalline

platinum [39], carbon supported Pt, Pt_3Ni and Pt_3Co alloys [40] and well-deffined Pt_3Co electrodes [9]. This, in turn, suggests that the reaction pathway on all these electrodes is identical.

Table 1: Kinetic parameters for the ORR on Pt and Pt bimetallic surfaces in 0.1M $HClO_4$ (*data for Pt_3Co taken from [9]):

Electrode	$\partial E/\partial \log(j_k)$ **mV/dec**		$\Delta H^{\#}$ **kJmol^{-1}** @η = **0.30V**	***m***	***n***
	293K lcd/hcd	**333K lcd/hcd**			
Pt (pc)	81/112	67/87	21	1	4
Pt_3Co^*-sputtered	74/107	55/77	22	1	4
Pt_3Co^*-annealed	81/105	61/77	25	1	4
Pt_3Ni-sputtered	86/113	54/78	23	1	4
Pt_3Ni-annealed	85/114	60/78	21	1	4

$\partial E/\partial \log(j_k)$ – Tafel slope; **lcd/hcd**- low/high current density
$\Delta H^{\#}$ - Activation energy
m **–** Reaction order
n – Number of electrons

The fact that Tafel slopes obtained for the Pt_3Ni and "Pt-skin" bimetallic surfaces are almost the same as for the pure Pt (see Table 1) is additional confirmation that the kinetics of the ORR on all these electrodes is governed by the same reaction mechanism, as will be discussed in section below. Inspection of Table 1 gives an important summary of the Tafel slopes for the ORR in $HClO_4$ on all surfaces: (i) two Tafel slopes can be extrapolated from potentiodynamic curves; (ii) Tafel plots are inversely proportional to the temperature, which is in agreement with results obtained on Pt(hkl) in alkaline solution [41], but opposite to measurements in H_2SO_4 where the Tafel plots are directly proportional to the temperature [38]. Recently published data from our group revealed that if the adsorption of oxygenated species on Pt (hkl) is controlled by the surface coverage of strongly adsorbed anions (e.g. Br^-, HSO_4^-), then the *j-E* relationship has an ideally temperature-dependent Tafel slope (-2 x 2.3(*RT/F*) [32;38]. In contrast, when adsorption of

oxygenated species on Pt electrodes is not affected by coadsorbing anions, e.g. as in alkaline solutions, then the $\partial \log j / \partial E$ relationship is inversely proportional to the *RT/F* term [41]. Based on the kinetic analysis of the polarization curves and from simulations of *log j-E* curves [41], it was proposed that the anomalous temperature behavior is a consequence of strong lateral repulsion between coadsorbed oxygenated species and the reaction intermediates (adsorption under Frumkin conditions). If we apply the same analogy in $HClO_4$ (note that perchlorate anions are negligibly adsorbed on Pt), decreasing of the "apparent" Tafel slopes with increasing temperature on all electrodes may indicate that the $\partial \log j / \partial E$ contains a significant contribution from the temperature dependent interaction of adsorbed oxygenated species under Frumkin conditions [41].

3.4 Reaction pathway

Given that essentially the same kinetic parameters are assessed from the analysis of experimental results for the ORR on all three surfaces, than it appears reasonable to propose that the reaction mechanism on all surfaces is the *same* as one proposed for pure Pt, *i.e.,* a "series" $4e^-$ reduction pathway which can be presented schematically as [32;38;42]:

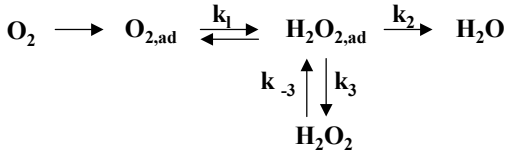

The first step is the adsorption of O_2 on the Pt available sites,

$$O_2 \rightarrow O_{2(ad)} \qquad (4)$$

that is followed by the rate determining step [43],

$$O_{2(ad)} + e^- \rightarrow O_2^-{}_{(ad)} \qquad (5)$$

If the rate controlling step is the first charge transfer then, for the first order dependence of the ORR kinetics found in this work, the general rate expression can be given by Eq. 6 [32]:

$$I = nFKC_{O_2}(1 - y\Theta_{ad})^x \exp(-\beta FE/RT)\exp(-\gamma r\,\Theta_{ad})/RT) \qquad (6)$$

where ***n*** is the number of electrons, ***K*** is the rate constant, c_{O_2} is the concentration of O_2 in the solution, Θ_{ad} is the total surface coverage by adsorbed species (hydroxyl and anions), ***x*** is the order of active Pt sites, ***y***=1 is the number of Pt sites blocked by OH_{ad}, ***I*** is the observed current, ***E*** is the applied potential, β and γ are the symmetry factors (assumed to be ½), $r\Theta_{ad}$ is parameter characterizing the rate of change of the apparent standard free energy of adsorption with the surface coverage by adsorbing species, ***T*** is temperature, ***F*** is Faraday's constant and ***R*** is universal gas constant (already introduced before). In what follows we use this equation to discuss differences in catalytic activities between Pt and Pt_3Ni surfaces. Based on the experimental results from this study: (i) the onset of OH adsorption is inhibited on Pt_3Ni and in particular on "Pt-skin" electrodes relative to Pt, Figure 1 (ii) specific adsorption of perchloric acid anions is negligible on Pt atoms and (iii) kinetic parameters on all three surfaces are essentially the same (see Table 1) it appears that the kinetics of the ORR on Pt and Pt_3Ni(Co) alloy surfaces in $HClO_4$ is primarily determined with the potential dependent surface coverage of OH_{ad} species [32], *i.e.*, by the $(1-\Theta_{ad})$ term in Eq. 6. It should be noticed that in previous studies from other laboratories [44-50], it was proposed that the enhanced ORR activity on Pt-Ni (and Pt-Co) alloys may arise due one or more of the following effects: (i) modification of the electronic structure of Pt (5-d orbital vacancies); (ii) change in the physical structure of Pt (Pt-Pt bond distance and coordination number); (iii) roughening by dissolution of alloying components; (iv) adsorption of oxygen containing species from the electrolyte onto the Pt or alloying element; and/or (v) redox type processes involving the first row transition alloying elements, etc.

In order to demonstrate how $(1-\Theta_{ad})$ and energetic terms are affected by the segregation phenomenon, activities for the ORR obtained in this study and our previous article [9], expressed

as kinetic current densities by using Eq. 2, are summarized in Fig.4. Clearly, at the fixed electrode potential of 0.85 V *vs*. RHE, both "Pt-skin" surfaces exhibit unique high activity for the ORR. The catalytic improvement of the ORR on these surfaces vs. Pt is ca. factor of 4. This is not surprising result considering that similar chemistry of transition metals may induce the similar electronic properties of Pt. As mentioned above, pronounced activity is in agreement with inhibition of oxides formation on the former surfaces, *i.e.* could be expressed as a positive shift of more than 50 mV in oxidation potential relative to Pt.

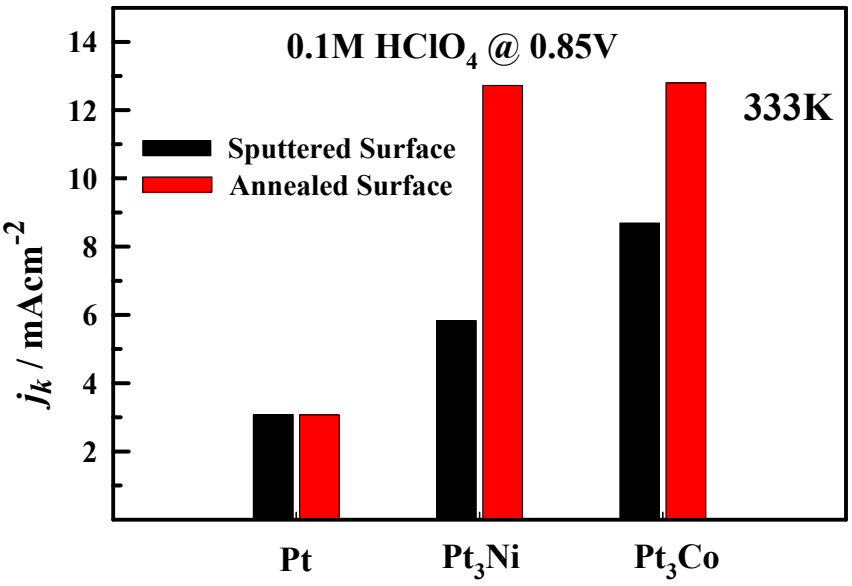

Figure 4. Histograms of the kinetic currents densities for the ORR at E= 0.85 V on Pt, Pt_3Ni, Pt_3Co and each "Pt-skin" surfaces at 333 K. Data for Pt_3Co surfaces are taken from the reference [9].

Thus we are proposing that the catalytic improvement of "Pt-skin" electrodes can be attributed to the weaker Pt-OH_{ad} interaction on electronically modified monoatomic layer of Pt atoms which are segregated on the top of the Ni (Co) enriched layer underneath. Some future theoretical aspects of the relationships between the electronic structure and reactivity could be useful in order to understand the trends in atomic/molecular chemisorption energies of oxygen containing species on the "Pt-skin" surfaces.

4. Conclusions:

The influence of surface segregation in a Pt_3Ni alloy has been studied for the ORR. Surfaces were prepared (annealing/sputtering cycles) and characterized (AES and LEISS) in UHV and then transferred into the electrochemical environment. Depending on a preparation method, two different surface compositions of Pt_3Ni electrode are produced: a sputtered surface with 75 % Pt and an annealed surface (950 K) with 100 % Pt. The cyclic voltammetry in 0.1 M $HClO_4$ solution of the 75 % Pt alloy surface, showed a decrease of H_{upd} pseudocapacitance (ca. 50 $\mu C/cm^2$) versus pure polycrystalline Pt surface, which was in agreement with the surface composition established by LEISS. No change of H_{upd} pseudocapacitance was observed on the "Pt-skin" electrode, confirming the outermost layer contains only Pt atoms. Catalytic activities of those two surfaces for the ORR were compared to the polycrystalline Pt in the temperature range of $298 < T < 333$ K. All the electrodes had stable *j-E* curves with consecutive cycling in potential range between 0.05-1.0 V at all temperatures. The order of activities at 333 K was "Pt-skin"> Pt_3Ni > Pt with the catalytic enhancement for the "Pt-skin" being 4 times higher than for pure Pt. Kinetic analyses on the Pt_3Ni and "Pt-skin" surfaces indicated nearly all kinetic parameters were the same as on pure Pt *e.g.* production of H_2O_2, the reaction order m=1, two identical Tafel slopes, the calculated activation energy, ≈ 20-25 kJ/mol. Only the pre-exponential factor is different. Essentially the same kinetic parameters on all three surfaces implies that the reaction mechanism on Pt_3Ni alloy surfaces is the same as the one proposed for the pure Pt, *i.e.*, a "series" $4e^-$ reduction pathway. For the Pt_3Ni electrode, catalytic enhancement was correlated to the inhibition of Pt-OH_{ad} formation *on* Pt sites surrounded by "oxide" covered Ni atoms. For the "Pt-skin" electrode catalytic improvement was attributed to the weaker Pt-OH_{ad} interaction on electronically modified monoatomic layer of Pt atoms which are segregated on the top of the Ni enriched layer underneath. The same level of catalytic enhancement was obtained for the "Pt-

skin" structure created on Pt_3Co alloy-reported earlier. Those improvements confirm unique properties of monolayer thin films and thus could be essential in the future design of high surface area catalysts for the fuel cells.

Acknowledgment:

This work was supported by the Assistant Secretary for Energy Efficiency and Renewable Energy, Office of Advance Transportation Technologies of the US Department of Energy under contract No.DE-AC03-76SF00098.

Reference List

1. A. P. Dowben and A. Miller, Surface segregation phenomena, CRC Press, Boca Raton, 1990.
2. P. N. Ross Jr., in J.Lipkowski and P.N.Ross Jr. (Eds.), Electrocatalysis, Wiley-VCH, Inc., New York, 1998, Ch. 2.
3. H. A. Gasteiger, N. Markovic, and P. N. Ross, J. Phys. Chem., 99 (1995) 16757-16767.
4. H. A. Gasteiger, N. M. Markovic, and P. N. Ross Jr., Catal. Let., 36 (1996) 1-8.
5. N. M. Markovic and P. N. Ross, Surf. Sci. Reports, 45 (2002) 121-254.
6. M. Polak and L. Rubinovich, Surface Science Reports, 262 (1999) 1-68.
7. J. K. Strohl and T. S. King, J. Catal, 116 (1989) 540.
8. N. M. Markovic and P. N. Ross, Electrochim. Acta, 45 (2000) 4101-4115.
9. V. Stamenkovic, T. J. Schmidt, N. M. Markovic, and P. N. Ross Jr., J. Phys. Chem. B, in press.
10. M. A. Vasiliev, J. Phys. D: Appl. Phys., 30 (1997) 3037-3070.
11. P. R. Watson, M. A. Van Hove, and K. Herman. Atlas of surface stucture. [Volum IA, Monograph 5]. 1995. Washington,DC, ACS Publications.
12. H. A. Gasteiger, N. Markovic, P. N. Ross, and E. J. Cairns, J. Phys. Chem., 97 (1993) 12020-12029.
13. N. M. Markovic, B. N. Grgur, and P. N. Ross Jr., J. Phys. Chem. B, 101 (1997) 5405-5413.

14. Y. Gauthier, Surf. Rev. and Letters, 3 (2001) 1663-1689.

15. Y. Gauthier, R. Baudoing, and J. Rundgren, Phys. Rev. B, 31 (1985) 6216-6218.

16. U. Bardi, A. Atrei, E. Zanazzi, G. Rovida, and P. N. Ross Jr., Vacuum, 41 (1990) 437-440.

17. Y. Gauthier, R. Baudoing-Savois, J. M. Bugnard, U. Bardi, and A. Atrei, Surf. Sci., 276 (1992) 1-11.

18. P. Beccat, Y. Gauthier, R. Baudoing, and J. C. Bertolini, Surf. Sci., 238 (1990) 105.

19. M. Ahmad and T. Tsong, Surf. Sci., 149 (1985) L7.

20. D. Ren and T. Tsong, Surf. Sci., 184 (1987) L439.

21. U. Bardi, B. Beard, and P. N. Ross, J. Catal, 124 (1990) 22.

22. D. P. Smith, J. Appl. Phys., 38 (1967) 340-347.

23. E. Taglauer, Appl. Phys. A, 38 (1985) 161-170.

24. G. Jerkiewicz, Progress in Surface Science, 57 (1998) 137-186.

25. N. M. Markovic, T. J. Schmidt, B. N. Grgur, H. A. Gasteiger, P. N. Ross Jr., and R. J. Behm, J. Phys. Chem. B, 103 (1999) 8568-8577.

26. T. J. Schmidt, U. A. Paulus, H. A. Gasteiger, N. Alonso-Vante, and R. J. Behm, J. Electrochem. Soc., 147 (1999)2620-2624.

27. M. R. Tarasevich, Electrochimiya, 9 (1973) 578.

28. M. R. Tarasevich and V. S. Vilinskaya, Electrochimiya, 9 (1973) 96.

29. F. Uribe, M. S. Wilson, T. Springer, and S. Gottesfeld, The Electrochemical Society. Proceedings of the Workshop on Structural Effetcs in Electrocatalytsis and Oxygen Electrochemistry. Ed.: Scherson, D., Tryk, D., Daroux, M., and Xing, X. 10-29-1991. Pennington, NJ, 1992.

30. R. R. Adzic, The Electrochemical Society. Proceedings of the Workshop on Structural Effetcs in Electrocatalytsis and Oxygen Electrochemistry. Ed.: Scherson, D., Tryk, D., Daroux, M., and Xing, X. 10-29-1991. Pennington, NJ, 1992.

31. N. M. Markovic, H. A. Gasteiger, and P. N. Ross, J. Phys. Chem., 100 (1996) 6715-6721.

32. N. M. Markovic, H. A. Gasteiger, B. N. Grgur, and P. N. Ross, J. Electroanal. Chem., 467 (1999) 157-163.

33. W. J. Albery and M. L. Hitchman, Ring-Disc Electrodes, Clarendon Press, Oxford, 1971.

34. Handbook of Chemistry and Physics in R.C.Weast (Ed.), CRC Press, Boca Raton, FL, 1986.

35. A. Schumpe, I. Adler, and W.-D. Deckwer, Biotechnol. Bioeng., 20 (1978) 145.

36. N. A. Anastasijevic, Z. M. Dimitrijevic, and R. R. Adzic, Electrochim. Acta, 31 (1986) 1125-1130.

37. N. M. Markovic, R. R. Adzic, B. D. Cahan, and E. Yeager, J. Electroanal. Chem., 377 (1994) 249-259.

38. B. N. Grgur, N. M. Markovic, and P. N. Ross Jr., Can. J. Chem., 75 (1997) 1465-1471.

39. A. Damjanovic and D. B. Sepa, Electrochim. Acta, 35 (1990) 1157-1162.

40. U. A. Paulus, G. G. Scherer, A. Wokaun, T. J. Schmidt, V. Stamenkovic, V. Radmilovic, N. M. Markovic, and P. N. Ross, J. Phys. Chem. B, 106 (2001) 4181-4191.

41. T. J. Schmidt, V. Stamenkovic, M. Arenz, N. M. Markovic, and P. N. Ross, Electrochim. Acta, 47 (2002) 3765-3776.

42. V. Stamenkovic, N. M. Markovic, and P. N. Ross Jr., J. Electroanal. Chem., 500 (2000) 44-51.

43. M. R. Tarasevich, A. Sadkowski, and E. Yeager, in Comprehensive Treatise in Electrochemistry, Ed.: J.O.M.Bockris, B.E.Conway, E.Yeager, S.U.M.Khan, and R.E.White, Plenum Press, New York, 1983, Ch. 6.

44. F. J. Luczak and D. A. Landsman. Ordered Ternary Fuel Cell Catalysts Containing Platinum, Cobalt and Chromium. 1984. US patent No. 4.447.506

45. C. A. Lucas, N. M. Markovic, and P. N. Ross, Phys. Rev. B, 55 (1997) 7964-7971.

46. F. J. Luczak and D. A. Landsman. Ordered Ternary Fuel Cell Catalysts Containing Platinum and Cobalt and Method for Making the Catalyst. 1987. US patent No. 4.677.092

47. B. Beard and P. N. Ross Jr., J. Electrochem. Soc., 137 (1990) 3368.

48. J. T. Glass, G. L. Cahen, and G. E. Stoner, J. Electrochem. Soc., 134 (1987) 58.

49. S. Mukerjee and S. Srinivasan, J. Electroanal. Chem., 357 (1993) 201.

50. T. Toda, H. Igarashi, H. Uchida, and M. Watanabe, J. Electrochem. Soc., 141 (1999) 968.